FERMILAB-PUB-09-649-E-PPD

Search for the Standard Model Higgs Boson in the $ZH \to \nu\bar{\nu}b\bar{b}$ Channel in 5.2 fb^{-1} of $p\bar{p}$ Collisions at $\sqrt{s} = 1.96$ TeV

V.M. Abazov[37], B. Abbott[75], M. Abolins[64], B.S. Acharya[30], M. Adams[50], T. Adams[48], E. Aguilo[6], G.D. Alexeev[37], G. Alkhazov[41], A. Alton[64,a], G. Alverson[62], G.A. Alves[2], L.S. Ancu[36], M. Aoki[49], Y. Arnoud[14], M. Arov[59], A. Askew[48], B. Åsman[42], O. Atramentov[67], C. Avila[8], J. BackusMayes[82], F. Badaud[13], L. Bagby[49], B. Baldin[49], D.V. Bandurin[58], S. Banerjee[30], E. Barberis[62], A.-F. Barfuss[15], P. Baringer[57], J. Barreto[2], J.F. Bartlett[49], U. Bassler[18], D. Bauer[44], S. Beale[6], A. Bean[57], M. Begalli[3], M. Begel[73], C. Belanger-Champagne[42], L. Bellantoni[49], J.A. Benitez[64], S.B. Beri[28], G. Bernardi[17], R. Bernhard[23], I. Bertram[43], M. Besançon[18], R. Beuselinck[44], V.A. Bezzubov[40], P.C. Bhat[49], V. Bhatnagar[28], G. Blazey[51], S. Blessing[48], K. Bloom[66], A. Boehnlein[49], D. Boline[61], T.A. Bolton[58], E.E. Boos[39], G. Borissov[43], T. Bose[61], A. Brandt[78], R. Brock[64], G. Brooijmans[70], A. Bross[49], D. Brown[19], X.B. Bu[7], D. Buchholz[52], M. Buehler[81], V. Buescher[25], V. Bunichev[39], S. Burdin[43,b], T.H. Burnett[82], C.P. Buszello[44], P. Calfayan[26], B. Calpas[15], S. Calvet[16], E. Camacho-Pérez[34], J. Cammin[71], M.A. Carrasco-Lizarraga[34], E. Carrera[48], B.C.K. Casey[49], H. Castilla-Valdez[34], S. Chakrabarti[72], D. Chakraborty[51], K.M. Chan[55], A. Chandra[53], E. Cheu[46], S. Chevalier-Théry[18], D.K. Cho[61], S.W. Cho[32], S. Choi[33], B. Choudhary[29], T. Christoudias[44], S. Cihangir[49], D. Claes[66], J. Clutter[57], M. Cooke[49], W.E. Cooper[49], M. Corcoran[80], F. Couderc[18], M.-C. Cousinou[15], D. Cutts[77], M. Ćwiok[31], A. Das[46], G. Davies[44], K. De[78], S.J. de Jong[36], E. De La Cruz-Burelo[34], K. DeVaughan[66], F. Déliot[18], M. Demarteau[49], R. Demina[71], D. Denisov[49], S.P. Denisov[40], S. Desai[49], H.T. Diehl[49], M. Diesburg[49], A. Dominguez[66], T. Dorland[82], A. Dubey[29], L.V. Dudko[39], L. Duflot[16], D. Duggan[67], A. Duperrin[15], S. Dutt[28], A. Dyshkant[51], M. Eads[66], D. Edmunds[64], J. Ellison[47], V.D. Elvira[49], Y. Enari[17], S. Eno[60], H. Evans[53], A. Evdokimov[73], V.N. Evdokimov[40], G. Facini[62], A.V. Ferapontov[77], T. Ferbel[60,71], F. Fiedler[25], F. Filthaut[36], W. Fisher[64], H.E. Fisk[49], M. Fortner[51], H. Fox[43], S. Fuess[49], T. Gadfort[73], C.F. Galea[36], A. Garcia-Bellido[71], V. Gavrilov[38], P. Gay[13], W. Geist[19], W. Geng[15,64], D. Gerbaudo[68], C.E. Gerber[50], Y. Gershtein[67], D. Gillberg[6], G. Ginther[49,71], G. Golovanov[37], B. Gómez[8], A. Goussiou[82], P.D. Grannis[72], S. Greder[19], H. Greenlee[49], Z.D. Greenwood[59], E.M. Gregores[4], G. Grenier[20], Ph. Gris[13], J.-F. Grivaz[16], A. Grohsjean[18], S. Grünendahl[49], M.W. Grünewald[31], F. Guo[72], J. Guo[72], G. Gutierrez[49], P. Gutierrez[75], A. Haas[70,c], P. Haefner[26], S. Hagopian[48], J. Haley[62], I. Hall[64], L. Han[7], K. Harder[45], A. Harel[71], J.M. Hauptman[56], J. Hays[44], T. Hebbeker[21], D. Hedin[51], J.G. Hegeman[35], A.P. Heinson[47], U. Heintz[77], C. Hensel[24], I. Heredia-De La Cruz[34], K. Herner[63], G. Hesketh[62], M.D. Hildreth[55], R. Hirosky[81], T. Hoang[48], J.D. Hobbs[72], B. Hoeneisen[12], M. Hohlfeld[25], S. Hossain[75], P. Houben[35], Y. Hu[72], Z. Hubacek[10], N. Huske[17], V. Hynek[10], I. Iashvili[69], R. Illingworth[49], A.S. Ito[49], S. Jabeen[61], M. Jaffré[16], S. Jain[69], D. Jamin[15], R. Jesik[44], K. Johns[46], C. Johnson[70], M. Johnson[49], D. Johnston[66], A. Jonckheere[49], P. Jonsson[44], A. Juste[49,d], E. Kajfasz[15], D. Karmanov[39], P.A. Kasper[49], I. Katsanos[66], V. Kaushik[78], R. Kehoe[79], S. Kermiche[15], N. Khalatyan[49], A. Khanov[76], A. Kharchilava[69], Y.N. Kharzheev[37], D. Khatidze[77], M.H. Kirby[52], M. Kirsch[21], J.M. Kohli[28], A.V. Kozelov[40], J. Kraus[64], A. Kumar[69], A. Kupco[11], T. Kurča[20], V.A. Kuzmin[39], J. Kvita[9], D. Lam[55], S. Lammers[53], G. Landsberg[77], P. Lebrun[20], H.S. Lee[32], W.M. Lee[49], A. Leflat[39], J. Lellouch[17], L. Li[47], Q.Z. Li[49], S.M. Lietti[5], J.K. Lim[32], D. Lincoln[49], J. Linnemann[64], V.V. Lipaev[40], R. Lipton[49], Y. Liu[7], Z. Liu[6], A. Lobodenko[41], M. Lokajicek[11], P. Love[43], H.J. Lubatti[82], R. Luna-Garcia[34,e], A.L. Lyon[49], A.K.A. Maciel[2], D. Mackin[80], P. Mättig[27], R. Magaña-Villalba[34], P.K. Mal[46], S. Malik[66], V.L. Malyshev[37], Y. Maravin[58], J. Martínez-Ortega[34], R. McCarthy[72], C.L. McGivern[57], M.M. Meijer[36], A. Melnitchouk[65], L. Mendoza[8], D. Menezes[51], P.G. Mercadante[4], M. Merkin[39], A. Meyer[21], J. Meyer[24], R.K. Mommsen[45], N.K. Mondal[30], T. Moulik[57], G.S. Muanza[15], M. Mulhearn[81], O. Mundal[22], L. Mundim[3], E. Nagy[15], M. Naimuddin[29], M. Narain[77], R. Nayyar[29], H.A. Neal[63], J.P. Negret[8], P. Neustroev[41], H. Nilsen[23], H. Nogima[3], S.F. Novaes[5], T. Nunnemann[26], G. Obrant[41], C. Ochando[16], D. Onoprienko[58], J. Orduna[34], N. Osman[44], J. Osta[55], R. Otec[10], G.J. Otero y Garzón[1], M. Owen[45], M. Padilla[47], P. Padley[80], M. Pangilinan[77], N. Parashar[54], V. Parihar[77], S.-J. Park[24], S.K. Park[32], J. Parsons[70], R. Partridge[77], N. Parua[53], A. Patwa[73], B. Penning[49], M. Perfilov[39], K. Peters[45], Y. Peters[45], P. Pétroff[16], R. Piegaia[1], J. Piper[64], M.-A. Pleier[73], P.L.M. Podesta-Lerma[34,f], V.M. Podstavkov[49], M.-E. Pol[2], P. Polozov[38], A.V. Popov[40], M. Prewitt[80], D. Price[53], S. Protopopescu[73], J. Qian[63], A. Quadt[24], B. Quinn[65], M.S. Rangel[16], K. Ranjan[29], P.N. Ratoff[43], I. Razumov[40], P. Renkel[79], P. Rich[45], M. Rijssenbeek[72], I. Ripp-Baudot[19], F. Rizatdinova[76], S. Robinson[44], M. Rominsky[75], C. Royon[18], P. Rubinov[49], R. Ruchti[55], G. Safronov[38], G. Sajot[14], A. Sánchez-Hernández[34], M.P. Sanders[26],

B. Sanghi[49], G. Savage[49], L. Sawyer[59], T. Scanlon[44], D. Schaile[26], R.D. Schamberger[72], Y. Scheglov[41], H. Schellman[52], T. Schliephake[27], S. Schlobohm[82], C. Schwanenberger[45], R. Schwienhorst[64], J. Sekaric[57], H. Severini[75], E. Shabalina[24], V. Shary[18], A.A. Shchukin[40], R.K. Shivpuri[29], V. Simak[10], V. Sirotenko[49], P. Skubic[75], P. Slattery[71], D. Smirnov[55], G.R. Snow[66], J. Snow[74], S. Snyder[73], S. Söldner-Rembold[45], L. Sonnenschein[21], A. Sopczak[43], M. Sosebee[78], K. Soustruznik[9], B. Spurlock[78], J. Stark[14], V. Stolin[38], D.A. Stoyanova[40], J. Strandberg[63], M.A. Strang[69], E. Strauss[72], M. Strauss[75], R. Ströhmer[26], D. Strom[50], L. Stutte[49], P. Svoisky[36], M. Takahashi[45], A. Tanasijczuk[1], W. Taylor[6], B. Tiller[26], M. Titov[18], V.V. Tokmenin[37], D. Tsybychev[72], B. Tuchming[18], C. Tully[68], P.M. Tuts[70], R. Unalan[64], L. Uvarov[41], S. Uvarov[41], S. Uzunyan[51], P.J. van den Berg[35], R. Van Kooten[53], W.M. van Leeuwen[35], N. Varelas[50], E.W. Varnes[46], I.A. Vasilyev[40], P. Verdier[20], L.S. Vertogradov[37], M. Verzocchi[49], M. Vesterinen[45], D. Vilanova[18], P. Vint[44], P. Vokac[10], H.D. Wahl[48], M.H.L.S. Wang[71], J. Warchol[55], G. Watts[82], M. Wayne[55], G. Weber[25], M. Weber[49,g], M. Wetstein[60], A. White[78], D. Wicke[25], M.R.J. Williams[43], G.W. Wilson[57], S.J. Wimpenny[47], M. Wobisch[59], D.R. Wood[62], T.R. Wyatt[45], Y. Xie[49], C. Xu[63], S. Yacoob[52], R. Yamada[49], W.-C. Yang[45], T. Yasuda[49], Y.A. Yatsunenko[37], Z. Ye[49], H. Yin[7], K. Yip[73], H.D. Yoo[77], S.W. Youn[49], J. Yu[78], C. Zeitnitz[27], S. Zelitch[81], T. Zhao[82], B. Zhou[63], J. Zhu[72], M. Zielinski[71], D. Zieminska[53], L. Zivkovic[70], V. Zutshi[51], and E.G. Zverev[39]

(D0 Collaboration)

[1] *Universidad de Buenos Aires, Buenos Aires, Argentina*
[2] *LAFEX, Centro Brasileiro de Pesquisas Físicas, Rio de Janeiro, Brazil*
[3] *Universidade do Estado do Rio de Janeiro, Rio de Janeiro, Brazil*
[4] *Universidade Federal do ABC, Santo André, Brazil*
[5] *Instituto de Física Teórica, Universidade Estadual Paulista, São Paulo, Brazil*
[6] *Simon Fraser University, Burnaby, British Columbia, Canada; and York University, Toronto, Ontario, Canada*
[7] *University of Science and Technology of China, Hefei, People's Republic of China*
[8] *Universidad de los Andes, Bogotá, Colombia*
[9] *Center for Particle Physics, Charles University, Faculty of Mathematics and Physics, Prague, Czech Republic*
[10] *Czech Technical University in Prague, Prague, Czech Republic*
[11] *Center for Particle Physics, Institute of Physics, Academy of Sciences of the Czech Republic, Prague, Czech Republic*
[12] *Universidad San Francisco de Quito, Quito, Ecuador*
[13] *LPC, Université Blaise Pascal, CNRS/IN2P3, Clermont, France*
[14] *LPSC, Université Joseph Fourier Grenoble 1, CNRS/IN2P3, Institut National Polytechnique de Grenoble, Grenoble, France*
[15] *CPPM, Aix-Marseille Université, CNRS/IN2P3, Marseille, France*
[16] *LAL, Université Paris-Sud, IN2P3/CNRS, Orsay, France*
[17] *LPNHE, IN2P3/CNRS, Universités Paris VI and VII, Paris, France*
[18] *CEA, Irfu, SPP, Saclay, France*
[19] *IPHC, Université de Strasbourg, CNRS/IN2P3, Strasbourg, France*
[20] *IPNL, Université Lyon 1, CNRS/IN2P3, Villeurbanne, France and Université de Lyon, Lyon, France*
[21] *III. Physikalisches Institut A, RWTH Aachen University, Aachen, Germany*
[22] *Physikalisches Institut, Universität Bonn, Bonn, Germany*
[23] *Physikalisches Institut, Universität Freiburg, Freiburg, Germany*
[24] *II. Physikalisches Institut, Georg-August-Universität Göttingen, Göttingen, Germany*
[25] *Institut für Physik, Universität Mainz, Mainz, Germany*
[26] *Ludwig-Maximilians-Universität München, München, Germany*
[27] *Fachbereich Physik, University of Wuppertal, Wuppertal, Germany*
[28] *Panjab University, Chandigarh, India*
[29] *Delhi University, Delhi, India*
[30] *Tata Institute of Fundamental Research, Mumbai, India*
[31] *University College Dublin, Dublin, Ireland*
[32] *Korea Detector Laboratory, Korea University, Seoul, Korea*
[33] *SungKyunKwan University, Suwon, Korea*
[34] *CINVESTAV, Mexico City, Mexico*
[35] *FOM-Institute NIKHEF and University of Amsterdam/NIKHEF, Amsterdam, The Netherlands*
[36] *Radboud University Nijmegen/NIKHEF, Nijmegen, The Netherlands*
[37] *Joint Institute for Nuclear Research, Dubna, Russia*
[38] *Institute for Theoretical and Experimental Physics, Moscow, Russia*
[39] *Moscow State University, Moscow, Russia*

[40]*Institute for High Energy Physics, Protvino, Russia*
[41]*Petersburg Nuclear Physics Institute, St. Petersburg, Russia*
[42]*Stockholm University, Stockholm, Sweden, and Uppsala University, Uppsala, Sweden*
[43]*Lancaster University, Lancaster, United Kingdom*
[44]*Imperial College London, London SW7 2AZ, United Kingdom*
[45]*The University of Manchester, Manchester M13 9PL, United Kingdom*
[46]*University of Arizona, Tucson, Arizona 85721, USA*
[47]*University of California, Riverside, California 92521, USA*
[48]*Florida State University, Tallahassee, Florida 32306, USA*
[49]*Fermi National Accelerator Laboratory, Batavia, Illinois 60510, USA*
[50]*University of Illinois at Chicago, Chicago, Illinois 60607, USA*
[51]*Northern Illinois University, DeKalb, Illinois 60115, USA*
[52]*Northwestern University, Evanston, Illinois 60208, USA*
[53]*Indiana University, Bloomington, Indiana 47405, USA*
[54]*Purdue University Calumet, Hammond, Indiana 46323, USA*
[55]*University of Notre Dame, Notre Dame, Indiana 46556, USA*
[56]*Iowa State University, Ames, Iowa 50011, USA*
[57]*University of Kansas, Lawrence, Kansas 66045, USA*
[58]*Kansas State University, Manhattan, Kansas 66506, USA*
[59]*Louisiana Tech University, Ruston, Louisiana 71272, USA*
[60]*University of Maryland, College Park, Maryland 20742, USA*
[61]*Boston University, Boston, Massachusetts 02215, USA*
[62]*Northeastern University, Boston, Massachusetts 02115, USA*
[63]*University of Michigan, Ann Arbor, Michigan 48109, USA*
[64]*Michigan State University, East Lansing, Michigan 48824, USA*
[65]*University of Mississippi, University, Mississippi 38677, USA*
[66]*University of Nebraska, Lincoln, Nebraska 68588, USA*
[67]*Rutgers University, Piscataway, New Jersey 08855, USA*
[68]*Princeton University, Princeton, New Jersey 08544, USA*
[69]*State University of New York, Buffalo, New York 14260, USA*
[70]*Columbia University, New York, New York 10027, USA*
[71]*University of Rochester, Rochester, New York 14627, USA*
[72]*State University of New York, Stony Brook, New York 11794, USA*
[73]*Brookhaven National Laboratory, Upton, New York 11973, USA*
[74]*Langston University, Langston, Oklahoma 73050, USA*
[75]*University of Oklahoma, Norman, Oklahoma 73019, USA*
[76]*Oklahoma State University, Stillwater, Oklahoma 74078, USA*
[77]*Brown University, Providence, Rhode Island 02912, USA*
[78]*University of Texas, Arlington, Texas 76019, USA*
[79]*Southern Methodist University, Dallas, Texas 75275, USA*
[80]*Rice University, Houston, Texas 77005, USA*
[81]*University of Virginia, Charlottesville, Virginia 22901, USA*
[82]*University of Washington, Seattle, Washington 98195, USA and*

(Received 29 December 2009; published 18 February 2010)

A search is performed for the standard model Higgs boson in 5.2 fb^{-1} of $p\bar{p}$ collisions at $\sqrt{s} = 1.96$ TeV, collected with the D0 detector at the Fermilab Tevatron Collider. The final state considered is a pair of b jets and large missing transverse energy, as expected from $p\bar{p} \to ZH \to \nu\bar{\nu}b\bar{b}$ production. The search is also sensitive to the $WH \to \ell\nu b\bar{b}$ channel when the charged lepton is not identified. For a Higgs boson mass of 115 GeV, a limit is set at the 95% C.L. on the cross section multiplied by branching fraction for $[p\bar{p} \to (Z/W)H](H \to b\bar{b})$ that is a factor of 3.7 larger than the standard model value, consistent with the factor of 4.6 expected.

PACS numbers: 14.80.Bn, 13.85.Ni, 13.85.Qk, 13.85.Rm

The existence of the Higgs boson is the only fundamental element of the standard model (SM) that has yet to be confirmed. Its observation would be a key step in establishing the mechanism of electroweak symmetry breaking and mass generation. Associated ZH production in $p\bar{p}$ collisions, with $Z \to \nu\bar{\nu}$ and $H \to b\bar{b}$, is among the most sensitive processes for seeking a Higgs boson with a mass $m_H \lesssim 135$ GeV at the Fermilab Tevatron Collider [8]. The D0 Collaboration published a search for this process based on 0.9 fb^{-1} of integrated luminosity [9]. The CDF Collaboration recently released the results of a search using 2.1 fb^{-1} [10]. A lower limit of 114.4 GeV was set by

the LEP experiments on the mass of the Higgs boson from searches for the reaction $e^+e^- \to ZH$ [11], while an indirect upper limit of 157 GeV can be inferred from precision electroweak data [12]. These limits and those given below are all defined at the 95% C.L.

This Letter presents a new search using an integrated luminosity more than 5 times larger than in [9]. The final-state topology considered consists of a pair of b jets from $H \to b\bar{b}$ and missing transverse energy ($\not\!\!E_T$) from $Z \to \nu\bar{\nu}$. The search is therefore also sensitive to the WH process when the charged lepton from $W \to \ell\nu$ decay is not identified. The main backgrounds arise from (W/Z)+heavy flavor jets (jets initiated by b and c quarks), top quark production, and multijet (MJ) events with $\not\!\!E_T$ arising from mismeasurement of jet energies.

The D0 detector is described in [13]. The data used in this analysis were recorded using triggers designed to select events with jets and $\not\!\!E_T$ [9, 14]. After imposing data quality requirements, the total integrated luminosity [15] is 5.2 fb^{-1}. The analysis relies on (i) charged particle tracks, (ii) calorimeter jets reconstructed in a cone of radius 0.5, using the iterative midpoint cone algorithm [16], and (iii) electrons or muons identified through the association of tracks with electromagnetic calorimeter clusters or with hits in the muon detector, respectively. The $\not\!\!E_T$ is reconstructed as the opposite of the vectorial sum of transverse components of energy deposits in the calorimeter and is corrected for identified muons. Jet energies are calibrated using transverse energy balance in photon+jet events [17], and these corrections are propagated to the $\not\!\!E_T$.

Backgrounds from SM processes are determined through Monte Carlo simulation, while instrumental MJ background is estimated from data. Events from (W/Z)+jets processes are generated with ALPGEN [18], interfaced with PYTHIA [19] for initial and final-state radiation and for hadronization. The p_T spectrum of the Z is reweighted to match the D0 measurement [20]. The p_T spectrum of the W is reweighted using the same experimental input, corrected for the differences between the Z and W p_T spectra predicted in next-to-next-to-leading order (NNLO) QCD [21]. For $t\bar{t}$ and electroweak single top quark production, the ALPGEN and COMPHEP [22] generators, respectively, are interfaced with PYTHIA, while vector boson pair production is generated with PYTHIA. The ZH and WH signal processes are generated with PYTHIA for Higgs boson masses (m_H) from 100 to 150 GeV, in 5 GeV steps. All these simulations use CTEQ6L1 parton distribution functions (PDFs) [23].

The absolute normalizations for (W/Z)+jets production are obtained from NNLO calculations of total cross sections based on [24], using the MRST2004 NNLO PDFs [25]. The heavy-flavor fractions are obtained using MCFM [26]. Cross sections for other SM backgrounds are taken from [27], or calculated with MCFM, and the cross sections for signal are taken from [28].

Signal and background samples are passed through a full GEANT3-based simulation [29] of detector response and processed with the same reconstruction program as used for data. Events from randomly selected beam crossings are overlaid on simulated events to account for detector noise and contributions from additional $p\bar{p}$ interactions. Parametrizations of trigger efficiency are determined using events collected with independent triggers based on information from the muon detectors. Weight factors compensating for residual differences between data and simulation are applied for electron, muon and jet identification. Jet energy calibration and resolution are adjusted in simulated events to match those measured in data.

A preselection that greatly reduces the overwhelming background from multijet events is performed as follows. The primary vertex must be reconstructed within the acceptance of the silicon vertex detector, and at least three tracks must originate from that vertex. Jets with associated tracks (using only tracks that meet minimal quality criteria to ensure that the b-tagging algorithm operates efficiently) are denoted as "taggable" jets. There must be two or three taggable jets, one of which is the leading (highest p_T) jet. These jets must have transverse momentum $p_T > 20$ GeV and pseudorapidity $|\eta| < 2.5$ [30]. The two leading taggable jets must not be back-to-back in the plane transverse to the beam direction: $\Delta\phi(\text{jet}_1, \text{jet}_2) < 165^\circ$. Finally, $\not\!\!E_T > 20$ GeV is required.

Additional selection criteria define four distinct samples: (i) an analysis sample used to search for a Higgs boson signal, (ii) an electroweak (EW) control sample, enriched in $W(\to \mu\nu)$+jets events where the jet system has a topology similar to that of the analysis sample, that is used to validate the SM background simulation, (iii) a "MJ-model" sample, dominated by multijet events, used to model the MJ background in the analysis sample, and (iv) a large "MJ-enriched" sample, used to validate this modeling procedure.

The analysis sample is selected by requiring $\not\!\!E_T > 40$ GeV and a measure of the $\not\!\!E_T$ significance $\mathcal{S} > 5$ [31]. Larger values of $\mathcal{S}$ correspond to $\not\!\!E_T$ values that are less likely to be caused by fluctuations in jet energies. In signal events, the missing track p_T, $\not\!\!p_T$, defined as the opposite of the vectorial sum of the charged particle transverse momenta, is expected to point in a direction close to that of $\not\!\!E_T$. Such a strong correlation is not expected in multijet events, where $\not\!\!E_T$ originates mainly from mismeasurement of jet energies. Advantage is taken of this feature by requiring $\mathcal{D} < \pi/2$, where $\mathcal{D} = \Delta\phi(\not\!\!E_T, \not\!\!p_T)$. Events containing an isolated electron or muon [32] with $p_T > 15$ GeV are rejected to reduce backgrounds from W+jets, top quark, and diboson production.

The EW-control sample is selected in a way similar to the analysis sample, except that an isolated muon with $p_T > 15$ GeV is required. The multijet content of

this sample is rendered negligible by requiring the transverse mass of the muon and $\not\!\!E_T$ system to be larger than 30 GeV. To ensure similar jet topologies for the analysis and EW-control samples, $\not\!\!E_T$ not corrected for the selected muon is required to exceed 40 GeV. Excellent agreement with the SM expectation is found for the number of selected events. The agreement for all kinematic distributions is also very good once a reweighting of the distribution of $\Delta\eta$ between the two leading taggable jets is performed, as suggested by a simulation of (W/Z)+jets using the SHERPA generator [33].

The MJ-model sample, used to determine the MJ background, is selected as the analysis sample, except that the requirement of $\mathcal{D} < \pi/2$ is inverted. The small contribution from non-MJ SM processes in the $\mathcal{D} > \pi/2$ region is subtracted, and the resulting sample is used to model the MJ background in the analysis sample. After adding contributions from SM backgrounds, the MJ background is normalized so that the expected number of events is identical to the number observed in the analysis sample.

The MJ-enriched sample is used to test the validity of this approach and is defined as the analysis sample, except that the $\not\!\!E_T$ threshold is reduced to 30 GeV and no requirement is imposed on $\mathcal{S}$. As a result, the MJ background dominates the entire range of $\mathcal{D}$ values, and this sample is used to verify that the events with $\mathcal{D} > \pi/2$ correctly model those with $\mathcal{D} < \pi/2$.

The large branching fraction for $H \to b\bar{b}$ is exploited by requiring that one or both of the two leading taggable jets be b tagged. The double-tag sample is selected with asymmetric requirements on the outputs of a b-tagging neural network algorithm [34], such that one jet is tagged with an efficiency of $\approx 70\%$ ("loose tag"), and the other with an efficiency of $\approx 50\%$ ("tight tag"). These values apply for taggable jets with $p_T \approx 45$ GeV and $|\eta| \approx 0.8$. The mistag rates , i.e., the probablilities to tag light (u, d, s, g) jets as b jets, are $\approx 6.5\%$ and $\approx 0.5\%$ for the loose and tight tags, respectively. The sensitivity of the search is improved by defining an independent single-tag sample in which one of the two leading taggable jets passes the tight tag and the other one fails the loose tag. The flavor-dependent b-tagging efficiencies are adjusted in simulated events to match those measured in dedicated data samples.

A boosted-decision-tree (DT) technique [35] takes advantage of different kinematics in signal and background processes. For each m_H, a "MJ DT" (multijet-rejection DT), used to discriminate between signal and MJ-model events, is trained before b tagging is applied, using 23 kinematic variables. These include the number of jets, jet p_T, dijet p_T, $\not\!\!E_T$, angles between jets, between dijet and $\not\!\!E_T$ and between jets and $\not\!\!E_T$, number of isolated tracks, and dijet mass, where the dijet system is constructed from the two leading taggable jets. The MJ-DT output (multijet discriminant) is shown in Fig. 1(a) for $m_H = 115$ GeV. A value of the multijet discriminant in excess of 0.6 is required (multijet veto), which removes over 95% of the multijet background and 65% of the non-MJ SM backgrounds, while retaining 70% of the signal. The number of expected signal and background events, as well as the number of observed events, are given in Table I after imposing the multijet veto.

To discriminate signal from SM backgrounds, additional "SM DTs" (SM rejection DTs) are trained separately for the single and double-tag samples, using the same kinematic variables as for the MJ DT. The outputs of the SM DTs after the multijet veto (final discriminants) are shown in Figs. 1(b) and 1(c) for $m_H = 115$ GeV, for the single and double tag samples.

Agreement between data and expectation from SM and MJ backgrounds is observed in the single and double tag samples, once the systematic uncertainties discussed below are taken into account, both in the number of selected events (Table I) and in distributions of final discriminants (Fig. 1). A modified frequentist approach [36] is used to set limits on the cross section for SM Higgs boson production, where the test statistic is a joint log-likelihood ratio (LLR) of the background-only and signal+background hypotheses, obtained by summing LLR values over the bins in the final discriminants shown in Figs. 1(b) and 1(c). The impact of systematic uncertainties on the sensitivity of the analysis is reduced by maximizing a "profile" likelihood function [37] in which these uncertainties are given Gaussian constraints associated with their priors.

Experimental uncertainties arise from trigger simulation (3%), jet energy calibration and resolution (3% for signal and $4\% - 5\%$ for background), jet reconstruction and taggability ($2\% - 3\%$), lepton identification ($1\% - 2\%$), and b tagging (from 2% for signal in the single-tag sample to 8% for background in the double-tag sample). Their impact is assessed on overall normalizations and shapes of distributions in final discriminants. Correlations among systematic uncertainties in signal and background are taken into account in extracting the final results, including a 6.1% uncertainty on the integrated luminosity.

Theoretical uncertainties on cross sections for SM processes are estimated as follows. For (W/Z)+jets production, an uncertainty of 6% is assigned to the total cross sections, and an uncertainty of 20% on the heavy-flavor fractions (estimated from MCFM). For other SM backgrounds, uncertainties are taken from [27] or from MCFM, and range from 6% to 10%. The uncertainties on cross sections for signal (6% for $m_H = 115$ GeV) are taken from [28]. Uncertainties on the shapes of the final discriminants arise from (i) the modeling of (W/Z)+jets, assessed by varying the renormalization-and-factorization scale and by comparing ALPGEN interfaced with HERWIG [38] to ALPGEN interfaced with PYTHIA, and (ii) the choice of PDFs, estimated using the prescription of [23]. The normalization of the MJ background is anticorrelated with the normalization of

TABLE I: The number of expected signal and background events, and the number observed after the multijet veto, prior to b tagging and for single and double tags. The signal corresponds to $m_H = 115$ GeV, "Top" includes pair and single top quark production, and VV is the sum of all diboson processes. The uncertainties quoted arise from the statistics of the simulation and from the sources of systematic uncertainties mentioned in the text.

Sample	ZH	WH	W+jets	Z+jets	Top	VV	Multijet	Total background	Observed
Pretag	13.73 ± 1.37	11.64 ± 1.17	19 069	9432	1216	1112	1196	32 025 ± 4121	31 718
Single tag	4.16 ± 0.42	3.60 ± 0.37	802	439	404	60	125	1830 ± 273	1712
Double tag	4.66 ± 0.58	4.00 ± 0.50	191	124	199	24	< 8	538 ± 93	514

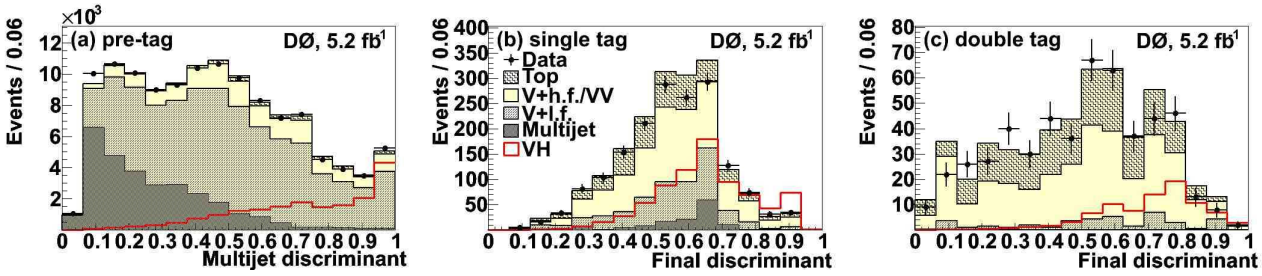

FIG. 1: Decision tree outputs for $m_H = 115$ GeV: (a) for the MJ DT, and for the SM DTs following the multijet veto for (b) single and (c) double tag. The data are shown as points with error bars. The background contributions are shown as histograms, with codes indicated in the legend in (b). Dibosons are labeled "VV," "V+l.f." includes $(W/Z)+(u,d,s,g)$ jets, "V+h.f." includes $(W/Z)+(b,c)$ jets, and "Top" includes pair and single top quark production. The distributions for signal (VH) are multiplied by factors of 500, 100, and 10 in (a)–(c), respectively.

the SM backgrounds, as the sum is constrained by data prior to b tagging.

The results of the analysis are given as limits in Table II and as LLRs in Fig. 2, as a function of m_H. The observed LLRs are within 1 standard deviation of expectation (the median of the LLR for the background-only hypothesis). For $m_H = 115$ GeV, the observed and expected limits on the combined cross section of ZH and WH production, multiplied by the branching fraction for $H \to b\bar{b}$, are factors of 3.7 and 4.6 larger than the SM value, respectively. These are the most constraining results for a SM Higgs boson decaying dominantly into $b\bar{b}$ for m_H above the limit set at LEP.

Supplementary material is provided in [39].

We thank the staffs at Fermilab and collaborating institutions, and acknowledge support from the DOE and NSF (USA); CEA and CNRS/IN2P3 (France); FASI, Rosatom and RFBR (Russia); CNPq, FAPERJ, FAPESP and FUNDUNESP (Brazil); DAE and DST (India); Colciencias (Colombia); CONACyT (Mexico); KRF and KOSEF (Korea); CONICET and UBACyT (Argentina); FOM (The Netherlands); STFC and the Royal Society (United Kingdom); MSMT and GACR (Czech Republic); CRC Program, CFI, NSERC and WestGrid Project (Canada); BMBF and DFG (Germany); SFI (Ireland); The Swedish Research Council (Sweden); and CAS and CNSF (China).

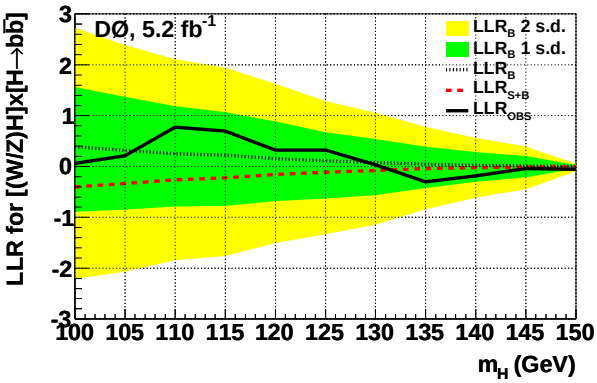

FIG. 2: The observed LLR is shown as a solid black line, the expected LLRs for the background-only and signal+background hypotheses are shown as black dots and red dashes, respectively, and the heavy green and light yellow shaded areas correspond to 1 and 2 standard deviations (s.d.) around the expected LLR for the background-only hypothesis.

[a] Visitor from Augustana College, Sioux Falls, SD, USA.
[b] Visitor from The University of Liverpool, Liverpool, UK.
[c] Visitor from SLAC, Menlo Park, CA, USA.
[d] Visitor from ICREA/IFAE, Barcelona, Spain.
[e] Visitor from Centro de Investigacion en Computacion - IPN, Mexico City, Mexico.
[f] Visitor from ECFM, Universidad Autonoma de Sinaloa,

TABLE II: As a function of m_H, observed and expected upper limits on the $(W/Z)H$ production cross section multiplied by branching fraction for $H \to b\bar{b}$, relative to the SM expectation.

m_H (GeV)	100	105	110	115	120	125	130	135	140	145	150
Observed	3.6	3.9	3.4	3.7	4.9	5.5	7.4	14.2	18.0	20.9	37.5
Expected	3.4	3.8	4.2	4.6	5.5	6.7	7.8	10.5	14.7	21.2	33.6

Culiacán, Mexico.

[g] Visitor from Universität Bern, Bern, Switzerland.

[8] M. Carena *et al.*, arXiv:hep-ph/0010338; CDF and D0 Collaborations, Report No. FERMILAB-PUB-03/320-E, 2003.

[9] V.M. Abazov *et al.* (D0 Collaboration), Phys. Rev. Lett. **101**, 251802 (2008).

[10] T. Aaltonen *et al.* (CDF Collaboration), arXiv:0911.3935.

[11] R. Barate *et al.* (LEP Working Group for Higgs boson searches), Phys. Lett. B **565**, 61 (2003).

[12] LEP, Tevatron and SLD Electroweak Working Groups, arXiv:0911.2604.

[13] V.M. Abazov *et al.* (D0 Collaboration), Nucl. Instrum. Methods Phys. Res., Sect. A **565**, 463 (2006); M. Abolins *et al.*, Nucl. Instrum. Methods Phys. Res., Sect. A **584**, 75 (2008); R. Angstadt *et al.*, arXiv:0911.2522.

[14] C. Ochando, Report No. FERMILAB-THESIS-2008-78.

[15] T. Andeen *et al.*, Report No. FERMILAB-TM-2365, 2007.

[16] G.C. Blazey *et al.*, arXiv:hep-ex/0005012.

[17] M. Voutilainen, Report No. FERMILAB-THESIS-2008-19.

[18] M.L. Mangano *et al.*, J. High Energy Phys. 07 (2003) 001; version 2.11 was used.

[19] T. Sjöstrand, S. Mrenna, and P. Skands, J. High Energy Phys. 05 (2006) 026; version 6.409 was used.

[20] V.M. Abazov *et al.*, (D0 Collaboration), Phys. Rev. Lett. **100**, 102002 (2008).

[21] K. Melnikov and F. Petriello, Phys. Rev. D **74**, 114017 (2006).

[22] E. Boos *et al.* (CompHEP Collaboration), Nucl. Instrum. Methods Phys. Res., Sect. A **534**, 250 (2004).

[23] J. Pumplin *et al.*, J. High Energy Phys. 07 (2002) 012; D. Stump *et al.*, J. High Energy Phys. 10 (2003) 046.

[24] R. Hamberg, W.L. van Neerven, and W.B. Kilgore, Nucl. Phys. **B359**, 343 (1991); **B644**, 403 (2002).

[25] A.D. Martin, R.G. Roberts, W.J. Stirling, and R.S. Thorne, Phys. Lett. B **604**, 61 (2004).

[26] J.M. Campbell and R.K. Ellis, Phys. Rev. D **60**, 113006 (1999).

[27] N. Kidonakis and R. Vogt, Phys. Rev. D **78**, 074005 (2008); N. Kidonakis, Phys. Rev. D **74**, 114012 (2006).

[28] T. Hahn *et al.*, arXiv:hep-ph/0607308.

[29] R. Brun and F. Carminati, CERN Program Library Long Writeup W5013, 1993 (unpublished).

[30] The pseudorapidity is defined as $\eta = -\ln[\tan(\theta/2)]$, where θ is the polar angle with respect to the proton beam direction.

[31] A. Schwartzman, Report No. FERMILAB-THESIS-2004-21.

[32] V.M. Abazov *et al.* (D0 Collaboration), Phys. Rev. D **76**, 092007 (2007).

[33] T. Gleisberg *et al.*, J. High Energy Phys. 02 (2004) 056; J. Alwall *et al.*, Eur. Phys. J. C **53**, 473 (2008).

[34] T. Scanlon, Report No. FERMILAB-THESIS-2006-43.

[35] L. Breiman *et al.*, *Classification and Regression Trees* (Wadsworth, Belmont, CA, 1984); Y. Freund and R.E. Schapire, in *Machine Learning: Proceedings of the Thirteenth International Conference, Bari, Italy, 1996,* edited by L. Saitta (Morgan Kaufmann, San Francisco, 1996), p148.

[36] T. Junk, Nucl. Instrum. Methods Phys. Res., Sect. A **434**, 435 (1999); A. Read, J. Phys. G **28**, 2693 (2002).

[37] W. Fisher, Report No. FERMILAB-TM-2386-E, 2006.

[38] G. Corcella *et al.*, J. High Energy Phys. 01 (2001) 010.

[39] See supplementary material appended for added information on event yields, DT variables, systematic uncertainties, for plots showing comparisons of data and predicted backgrounds, and for plots of the cross section limits.

Supplementary material

TABLE III: Theoretical cross sections for associated WH and ZH production and $H \to b\bar{b}$ branching fraction, as a function of m_H.

m_H (GeV)	100	105	110	115	120	125	130	135	140	145	150
$\sigma(WH)$ (pb)	0.286	0.243	0.208	0.178	0.153	0.132	0.115	0.099	0.087	0.076	0.066
$\sigma(ZH)$ (pb)	0.167	0.143	0.123	0.107	0.093	0.081	0.070	0.062	0.054	0.048	0.042
$B(H \to b\bar{b})$	0.812	0.796	0.770	0.732	0.679	0.610	0.527	0.436	0.344	0.256	0.176

TABLE IV: The number of observed events and the number of ZH and WH signal events expected for $m_H = 115$ GeV at different stages of the selection.

	Data	ZH	WH
Preselection	7690773	19.9	40.8
$\not\!\!E_T > 40$ GeV	790496	19.2	36.1
$\not\!\!E_T$ Significance > 5	188761	18.2	32.7
Isolated e/μ veto	153542	18.1	21.4
$\Delta\phi(\not\!\!E_T, \not\!\!p_T) < \pi/2$	120875	17.7	18.6

TABLE V: The number of expected signal and background events, and the number observed in the analysis sample before the multijet veto, prior to b tagging and for single and double tags; "top" includes pair and single top quark production. The quoted uncertainties are statistical only.

Sample	pre-tag	single tag	double tag
ZH (115 GeV)	17.72 ± 0.09	5.44 ± 0.05	5.69 ± 0.05
WH (115 GeV)	18.55 ± 0.15	5.81 ± 0.08	5.83 ± 0.07
W+jets	55502 ± 135	1311 ± 24	136 ± 10
W+b/c jets	9102 ± 46	1252 ± 15	411 ± 8
Z+jets	17785 ± 131	211 ± 17	9 ± 3
Z+b/c jets	4621 ± 36	701 ± 11	256 ± 6
top	2408 ± 6	815 ± 3	427 ± 2
di-boson	2309 ± 15	126 ± 3	42 ± 2
SM background	91727 ± 197	4415 ± 35	1282 ± 15
MJ background	29148 ± 377	2255 ± 101	398 ± 20
Total background	120875 ± 425	6670 ± 107	1679 ± 25
Observed	120875	6853	1581

TABLE VI: The number of expected signal and background events, and the number observed in the analysis sample after the multijet veto, prior to b tagging and for single and double tags; "top" includes pair and single top quark production. The quoted uncertainties are statistical only.

Sample	pre-tag	single tag	double tag
ZH (115 GeV)	13.73 ± 0.08	4.16 ± 0.05	4.66 ± 0.04
WH (115 GeV)	11.64 ± 0.12	3.60 ± 0.07	3.99 ± 0.06
W+jets	15997 ± 65	367 ± 12	38 ± 6
W+b/c jets	3072 ± 26	435 ± 8	153 ± 5
Z+jets	7304 ± 80	94 ± 12	2 ± 1
Z+b/c jets	2129 ± 24	344 ± 8	122 ± 4
top	1216 ± 4	404 ± 2	199 ± 2
di-boson	1112 ± 10	60 ± 2	24 ± 1
SM background	30829 ± 109	1704 ± 20	539 ± 9
MJ background	1196 ± 120	125 ± 32	-1 ± 8
Total background	32025 ± 162	1830 ± 38	538 ± 12
Observed	31718	1712	514

TABLE VII: Variables used as input to the Decision Trees.

Number of jets
Number of taggable jets
leading jet p_T
second jet p_T
third jet p_T
H_T(scalar sum of jet p_T)
$\Delta R(\mathrm{jet}_1, \mathrm{jet}_2)$
$\Delta\eta(\mathrm{jet}_1, \mathrm{jet}_2)$
$\Delta\phi(\mathrm{jet}_1, \mathrm{jet}_2)$
$\not\!\!E_T$
$\not\!\!E_T$ significance
$\Delta\phi(\not\!\!E_T, \mathrm{jet}_1)$
$\Delta\phi(\not\!\!E_T, \mathrm{jet}_2)$
$\Delta\phi(\not\!\!E_T, \text{dijet system})$
$\min \Delta\phi(\not\!\!E_T, \mathrm{jet_i})$
$\max \Delta\phi(\not\!\!E_T, \mathrm{jet_i}) + \min \Delta\phi(\not\!\!E_T, \mathrm{jet_i})$
$\max \Delta\phi(\not\!\!E_T, \mathrm{jet_i}) - \min \Delta\phi(\not\!\!E_T, \mathrm{jet_i})$
$\not\!\!H_T$(vectorial sum of jet p_T)
$\not\!\!H_T$/ H_T
dijet p_T
dijet mass
dijet transverse mass
Number of isolated tracks

TABLE VIII: Systematic uncertainties in % of the overall signal and background yields. "Jet EC" and "Jet ER" stand for jet energy calibration and resolution, respectively. "Jet R&T" stands for jet reconstruction and taggability. "Signal" includes ZH and WH production for $m_H = 115$ GeV.

Systematic Uncertainty	Signal	Background
pre-tag		
Jet EC – Jet ER	2.7	7.7
Jet R&T	3.0	3.7
Trigger	2.9	3.1
Lepton identification	1.0	1.1
Heavy-flavor fractions	–	2.6
Cross sections	6.0	6.3
Luminosity	6.1	5.9
Multijet normalization	–	0.9
Total	10.0	12.9
single tag		
Jet EC – Jet ER	2.6	4.7
Jet R&T	3.0	2.5
b tagging	1.9	5.2
Trigger	2.9	3.0
Lepton identification	1.0	1.2
Heavy-flavor fractions	–	8.1
Cross sections	6.0	7.1
Luminosity	6.1	5.7
Multijet normalization	–	1.8
Total	10.1	14.8
double tag		
Jet EC – Jet ER	2.8	3.6
Jet R&T	3.2	2.2
b tagging	7.3	8.0
Trigger	3.0	3.3
Lepton identification	1.1	1.6
Heavy-flavor fractions	–	9.8
Cross sections	6.0	8.0
Luminosity	6.1	6.1
Multijet normalization	–	0.4
Total	12.4	17.1

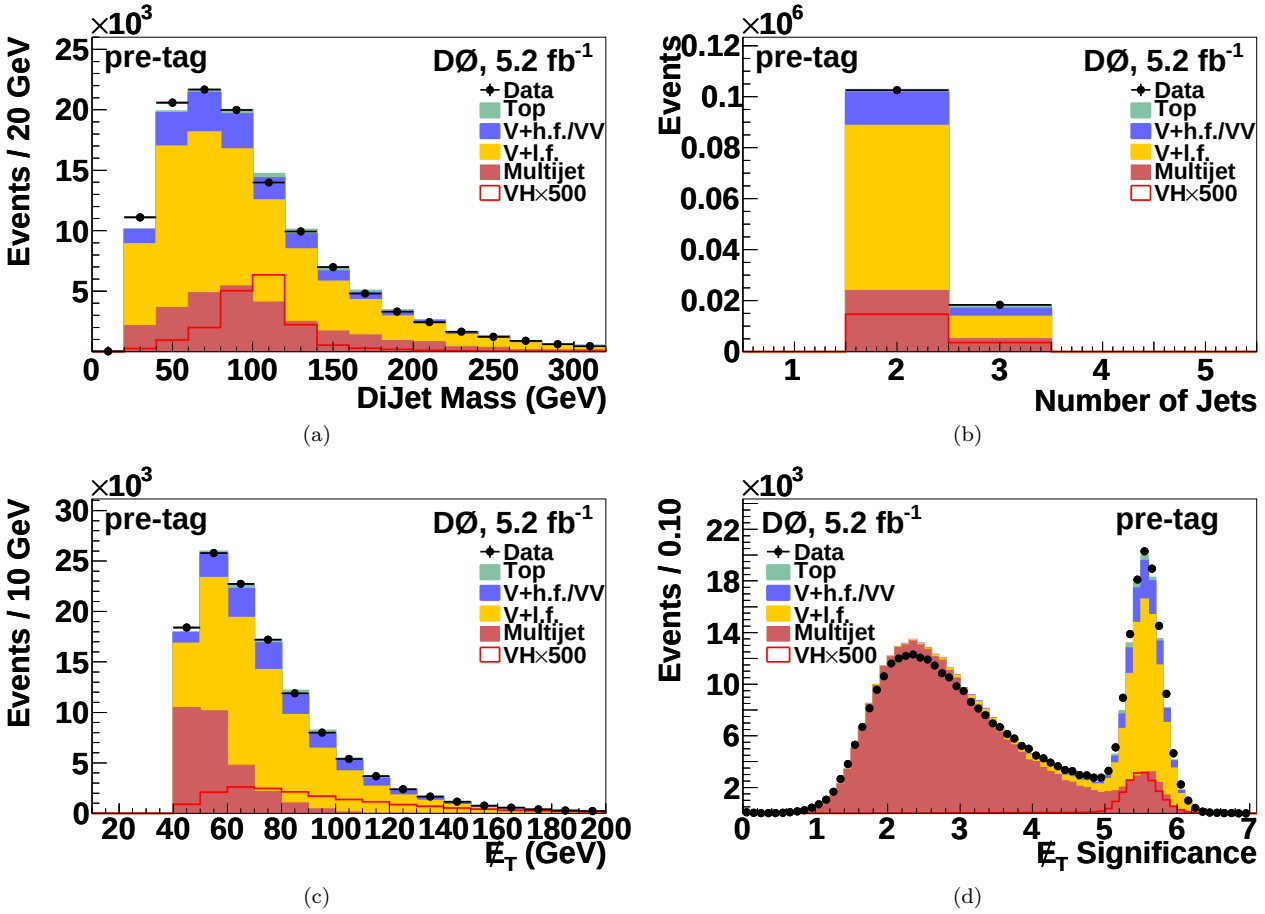

FIG. 3: Distributions in the analysis sample before the multijet veto: (a) Dijet invariant mass, (b) Taggable jet multiplicity, (c) Missing E_T, (d) Missing E_T significance without the requirement that it be larger than 5. The signal includes ZH and WH production for $m_H = 115$ GeV.

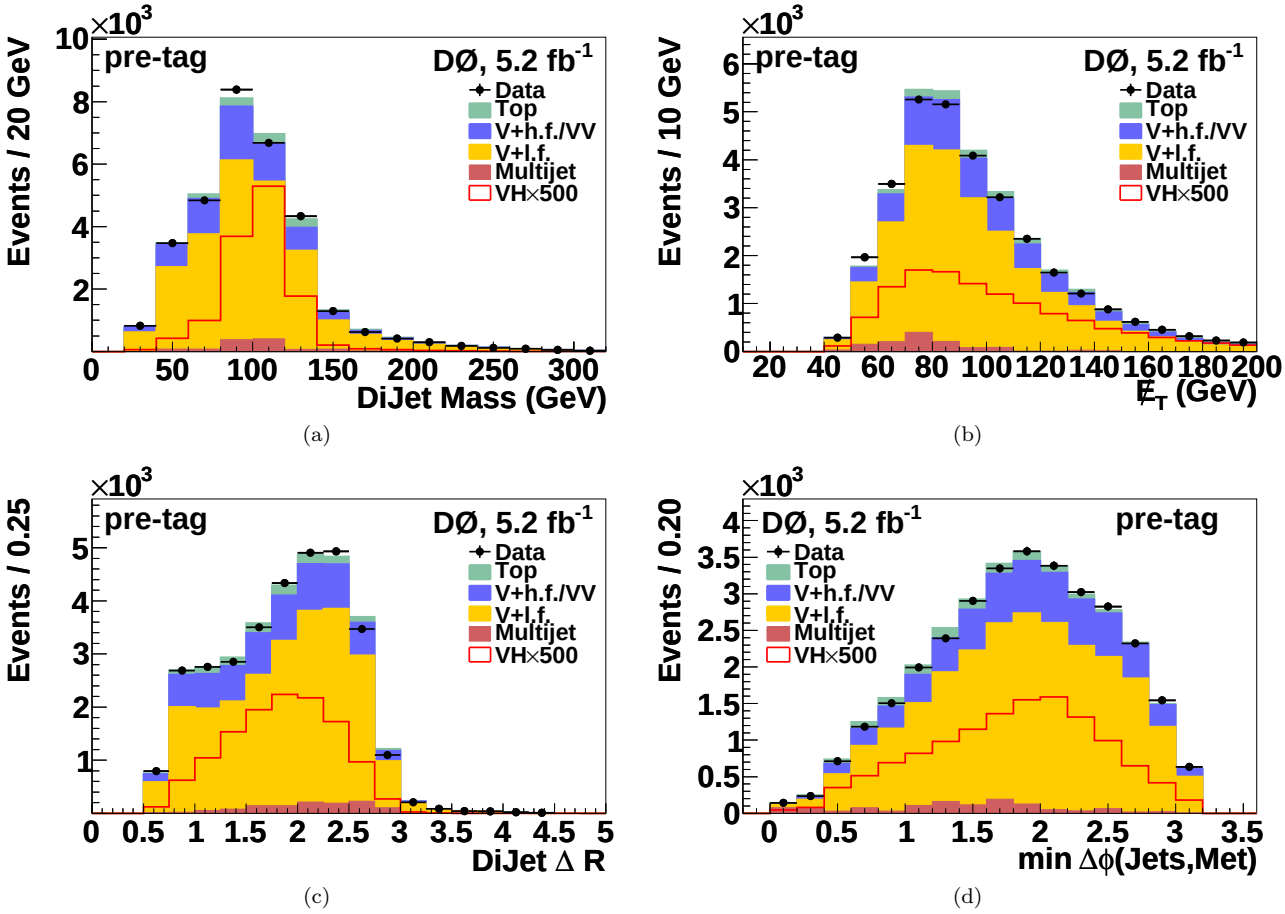

FIG. 4: Distributions in the analysis sample after the multijet veto: (a) Dijet invariant mass, (b) Missing E_T, (c) Dijet ΔR, (d) Minimum $\Delta\phi$ between any jet and $\not\!\!E_T$. The signal includes ZH and WH production for $m_H = 115$ GeV.

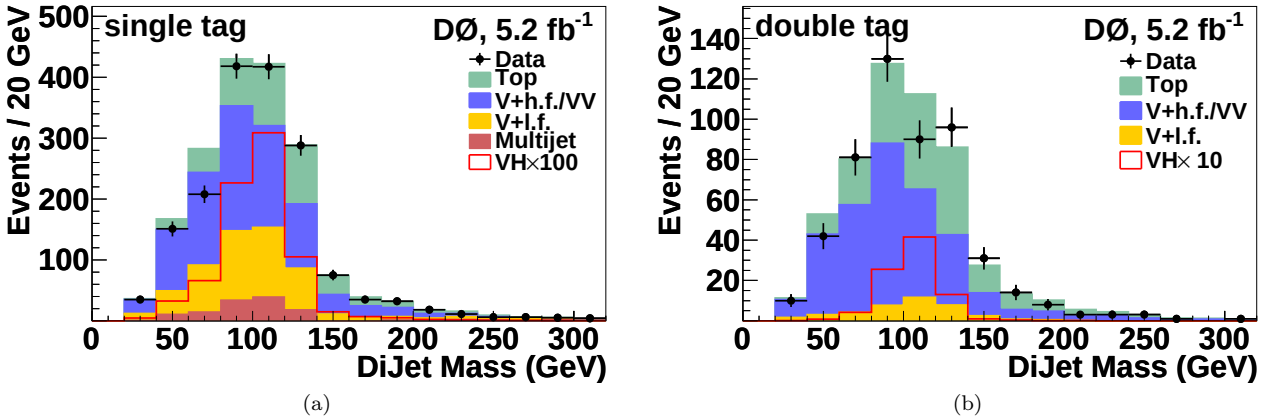

FIG. 5: Distributions in the analysis sample after the multijet veto: (a) Dijet invariant mass with single tag, (b) Dijet invariant mass with double tag. The signal includes ZH and WH production for $m_H = 115$ GeV.

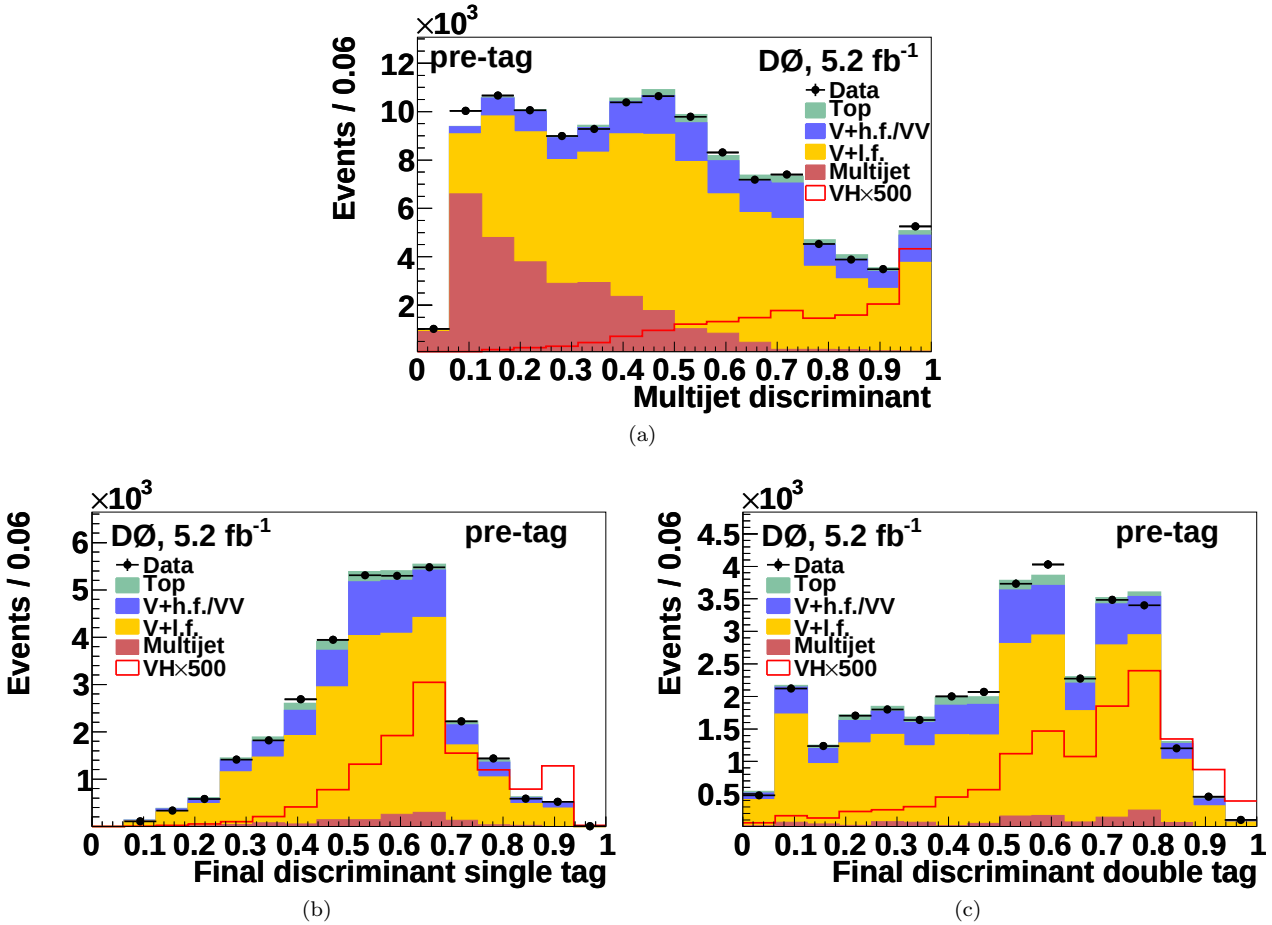

FIG. 6: Discriminants in the analysis sample: (a) Multijet discriminant, (b) Final single tag discriminant in the pre-tag sample, (c) Final double tag discriminant in the pre-tag sample. The signal includes ZH and WH production for $m_H = 115$ GeV.

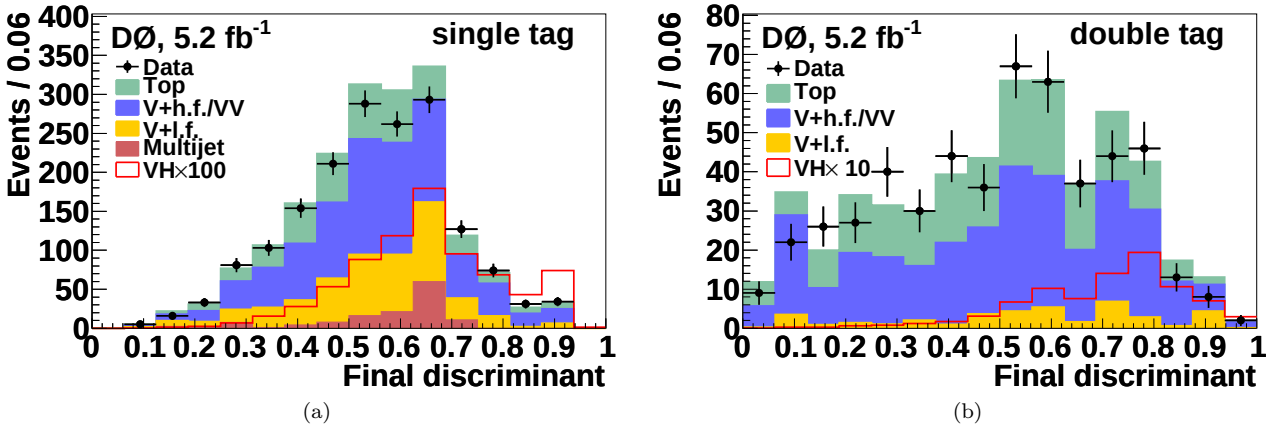

FIG. 7: Discriminants in the analysis sample: (a) Final single tag discriminant in the single tag sample, (b) Final double tag discriminant in the double tag sample. The signal includes ZH and WH production for $m_H = 115$ GeV.

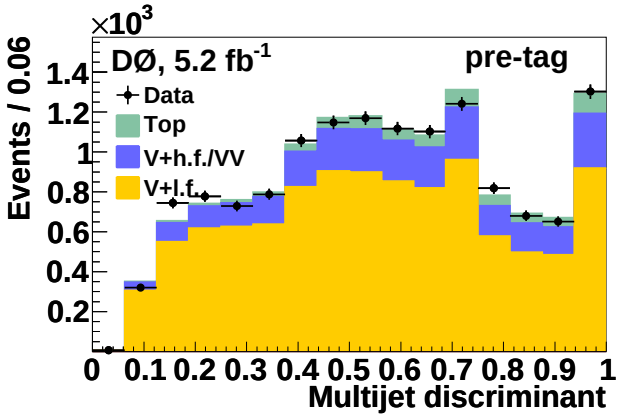

(a)

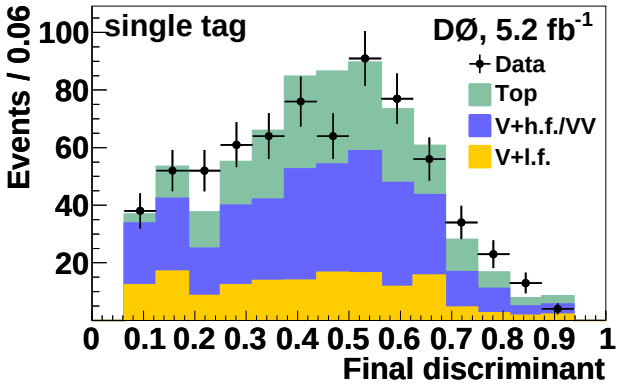

(b)

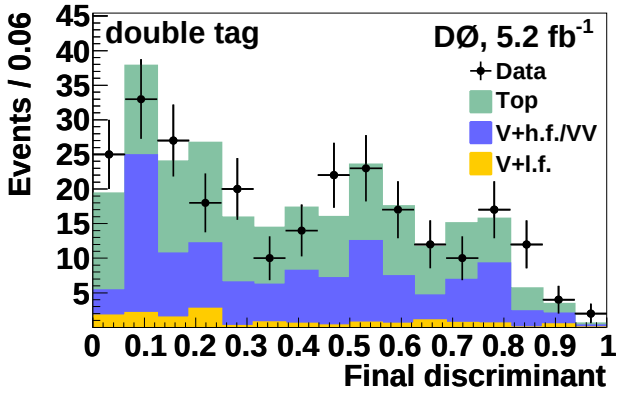

(c)

FIG. 8: Discriminants in the EW-control sample: (a) Multijet discriminant, (b) Final single tag discriminant in the single tag sample, (c) Final double tag discriminant in the double tag sample.

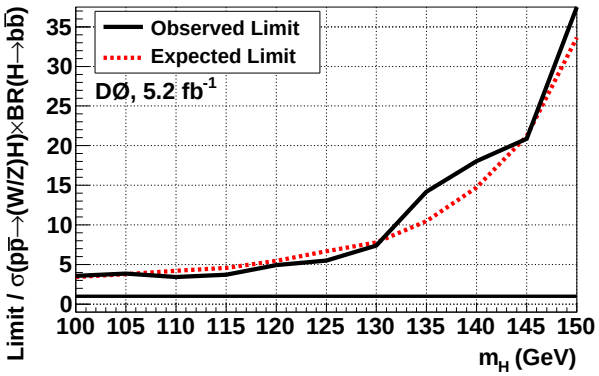

(a)

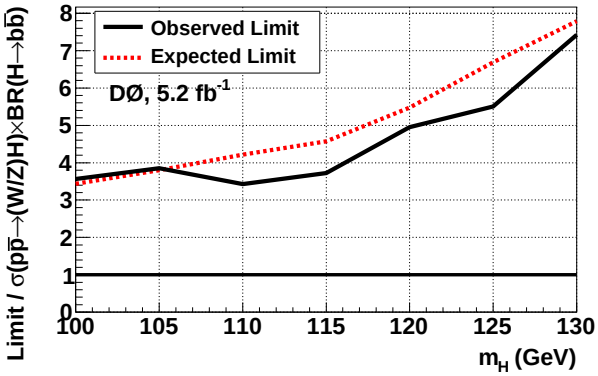

(b)

FIG. 9: (a) Ratio of the observed (solid black) and expected (dotted red) exclusion limits to the SM production cross section multiplied by branching fraction for $H \to b\bar{b}$, as a function of m_H, (b) The same zoomed in the low mass region.